# Tri-band four elements MIMO antenna system for WLAN and WiMAX application

R. Karimian [a], M. Soleimani [a] & S.M. Hashemi [a]

[a] Antenna and Microwave Research Laboratory, Department of
Electrical Engineering, Iran University of Science and Technology,
Tehran, 1684613114, Iran

**ᕗFirst**

PLEASE SCROLL DOWN FOR ARTICLE

# Tri-band four elements MIMO antenna system for WLAN and WiMAX application

R. Karimian*, M. Soleimani and S.M. Hashemi

*Antenna and Microwave Research Laboratory, Department of Electrical Engineering, Iran University of Science and Technology, Tehran 1684613114, Iran*

A new L-shaped slot dipole for multiple-input–multiple-output (MIMO) antenna system with an L-shaped slit is presented for WLAN and WiMAX applications. The L-shaped slot provides two bands at 2.4 and 5.2 GHz, and the third frequency at 3.5 GHz is achieved by introducing the L-shaped slit. The MIMO antenna consists of four symmetrical antenna elements. Each element is fed through a 50-Ω microstrip feed line-coupling electromagnetic field to the slot. A high isolation of 16 dB among the four antennas is achieved for an antenna spacing less than 0.05 λ. The MIMO structure gives high gain (>4.0 dB), low correlation (<0.05), and high radiation efficiency (>93%) The results indicate that the proposed MIMO antenna can provide spatial or pattern diversity to increase data capacity of wireless communication systems.

## 1. Introduction

Multiple-input–multiple-output (MIMO) systems have been the subject of investigation for several years. Demand for high data rate and large channel capacity of users in recent mobile communication systems drives the development of MIMO systems [1]. A practical MIMO antenna should have a low signal correlation between the antenna elements and good matching characteristic of input impedance [2,3]. In addition, since the isotropic pattern leads to an increase in channel capacity, it is desirable that all the elements have the same radiation and isotropic pattern, simultaneously. Moreover, reduction of mutual coupling among closely spaced antenna elements is severe and leads to weak MIMO system performance. Many studies have been done using MIMO antenna system [4–9]. Various techniques have been applied to reduce the mutual coupling between the elements [10–17]. In [10], two types of antenna elements printed on different sides of the substrate, with series of slits etched in the ground plane, were proposed to reduce mutual coupling between elements. In [11], the wideband T-shaped neutralization line, in [12], tree-like structure, and in [13], parasitic elements are the other techniques that have been used to enhance port-to-port isolation. Low mutual coupling can also be achieved through specific ground structure [14–16] and 180° coupler [17].

In this paper, a planar four-slot elements MIMO antenna with good isolation is presented. Each slot is proximity-fed by a 50-Ω microstrip line. The slot antennas are orthogonal with each other in order to realize polarization diversity. In general, the mutual coupling between two closely placed antennas is mainly caused by induced currents due to sharing common

---

*Corresponding author. Email: rezakarimian@elec.iust.ac.ir

ground and near-field coupling [18]. By separating the common ground plane of antenna structure and placing the antenna at the best-array configuration, high isolation (better than 16 dB) is achieved for antenna spacing even less than 0.05 $\lambda_0$, where $\lambda_0$ is the free space wavelength at the lower center frequency.

In comparison with [5], the proposed array offers enhanced performances in terms of operating frequency bands with better isolation between the elements in addition to the advantage of antenna efficiency and gain.

## 2.  Antenna structure and design

The designed and fabricated MIMO antenna structure is shown in Figures 1 and 2, respectively. A four-symmetrical dipole-slots antenna has been used in this structure. Each antenna consists of an L-shaped slot and an L-shaped slit that have been cut on the ground plan which is prox-imity-fed by a 50-$\Omega$ microstrip line, and the least edge to edge separation of the elements is 0.048 $\lambda_0$ at 2.4 GHz. It has been shown in [19] that the resonant frequency of an open slot on a ground plane is approximately $\lambda/2$, where $\lambda$ is the resonant wavelength. In order to design the tri-band antenna, the first L-shaped slot operating at resonant frequency of 2.4 GHz is cut on ground plan. The dimension of the L-shaped slot is $L_1 + L_2 = 61.7$ mm $\cong \lambda/2$. The second resonant frequency at 5.2 GHz is in the range of, $0.7 < L/\lambda < 0.9$. Creating the third resonant frequency of 3.5 GHz requires extra resonant mode that can be added by introducing an L-shaped slit on the ground plane. Figure 3 shows the simulated magnitude of the reflection coefficient of the proposed single antenna with and without the L-shaped slit. As marked in Figure 3, the equivalent impedance seen by the microstrip line at frequency of 3.9 GHz is 52-j58 $\Omega$. The L-shaped slit acts like a parallel capacitance; it has compensated the imaginary part of impedance, so a good matching in the frequency of 3.5 GHz is acquired [20].

In order to have a better understanding of the design procedure of the antenna, some para-metric studies and current distribution on the antenna have been investigated. Figure 4 depicts simulated magnitude of the reflection coefficient of antenna with different values of the slit's vertical position ($Ys$). Medial frequency changes with varying $Ys$, while the other frequencies are almost constant. Figure 5 shows that the magnitude of the reflection coefficient of the antenna in the two horizontal positions is approximately the same, because the equivalent capacity seen by the microstrip line is almost constant for the two positions. Figure 6(a) and (b) shows the surface current density and the $E$-field distribution at the frequency of 2.4 GHz, respectively. The ground currents flow around the slot edge in a manner the same as those on the conventional half-wavelength slot antenna. A peak value at the middle and two minimum
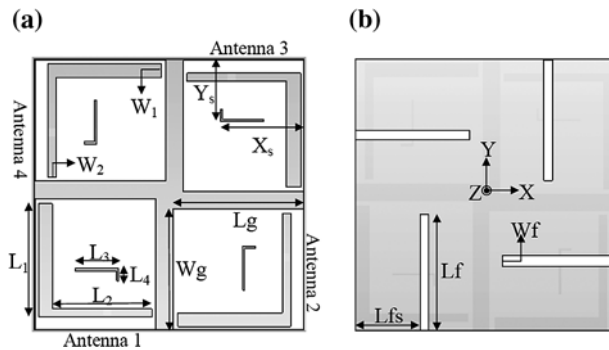
Figure 1.   Prototype of MIMO antenna system with four elements. (a) Top view and (b) bottom view.
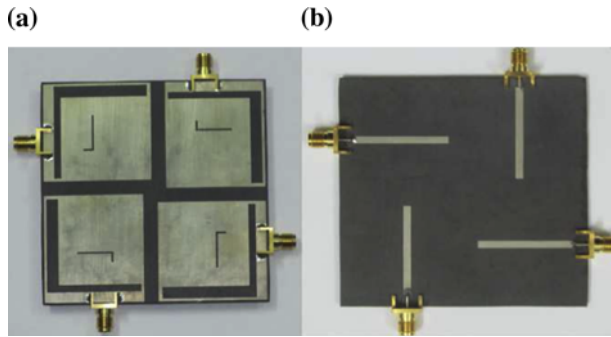
Figure 2.    Prototype of fabricated MIMO antenna. (a) Top view and (b) bottom view.
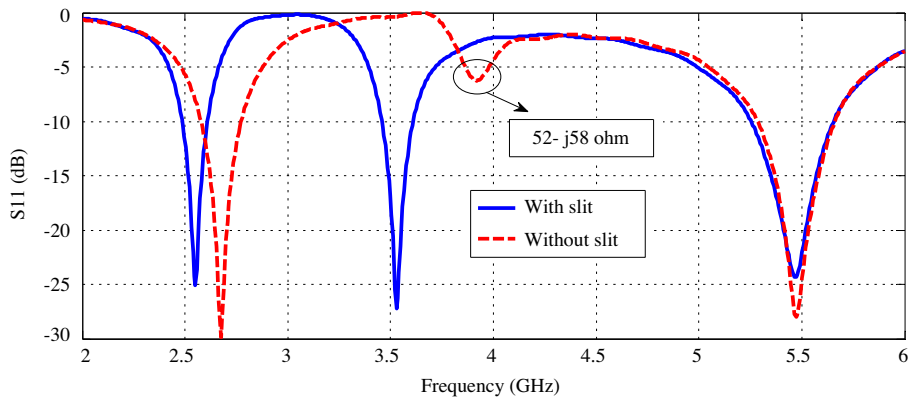


Figure 3.    Simulated magnitude of the reflection coefficient of proposed antenna with and without the L-shaped slit.



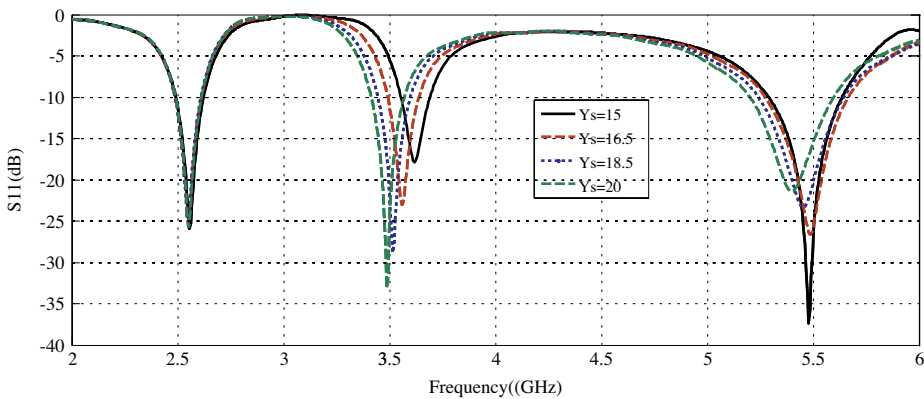Figure 4.    Simulated magnitude of the reflection coefficient with *Ys* variation.

values at the end of the L-shaped slot can be seen from *E*-field distribution. As expected and shown in Figure 7(a) and (b), the surface current path length at the frequency of 3.5 GHz is approximately 0.7$\lambda$ and at the frequency of 5.2 GHz is 0.9$\lambda$, where $\lambda$ is the wavelength at resonant frequency.
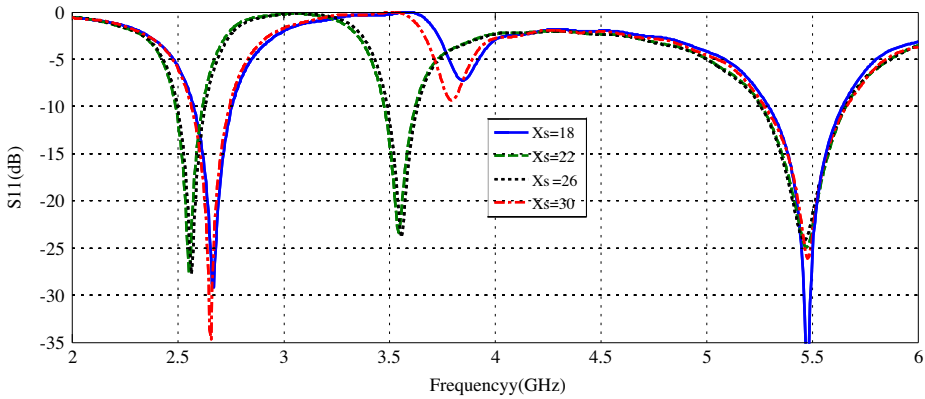
Figure 5.    Simulated magnitude of the reflection coefficient with *Xs* variation.
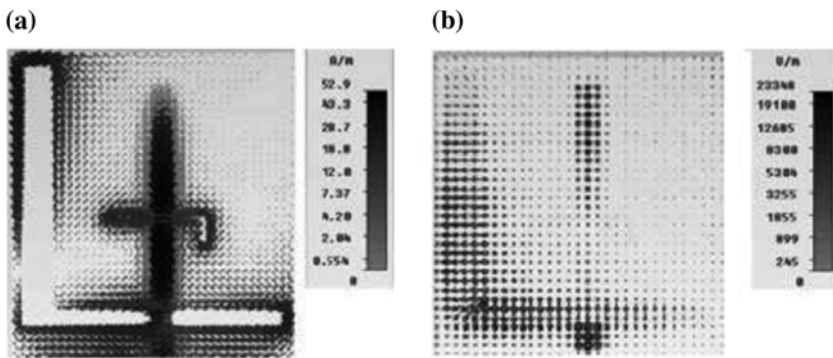


Figure 6.    Simulation of (a) surface current distribution and (b) *E*-field distribution at frequency of 2.4 GHz.
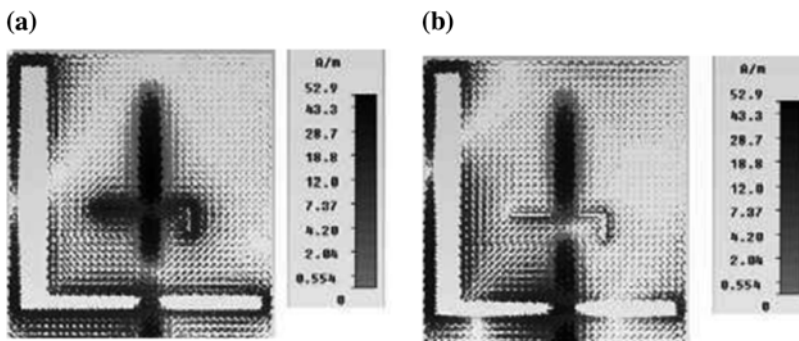


Figure 7.    Surface current distribution at the frequency of (a) 3.5 GHz and (b) 5.2 GHz.

The substrate dimension used for the proposed antenna is 35 mm × 38 mm, $h = 0.8$ mm thickness, and permittivity $\varepsilon_r = 2.2$. By fixing optimum parameters of the proposed antenna, good impedance matching through the operating bands for WLAN and WiMAX applications can be achieved. Table 1 summarizes the dimensions of the proposed antenna.

Table 1.   Dimensions of the proposed antenna (Unit: mm).

| $L_g$ | $W_g$ | $L_1$ | $L_2$ | $L_3$ | $L_4$ | $W_1$ | $W_2$ | $L_f$ | $L_{fs}$ | $W_f$ | $X_s$ | $Y_s$ |
|---|---|---|---|---|---|---|---|---|---|---|---|---|
| 38 | 35 | 32.8 | 28.9 | 12.6 | 3.6 | 4 | 2.38 | 34.3 | 19.75 | 2.48 | 24.3 | 17.8 |

## 3.   Antenna performance

### 3.1.   *Impedance performance*

The comparison between simulated and measured return–loss characteristics of the proposed antenna obtained by using CST 2010 and Agilent E8361C vector network analyzer is shown in Figure 8. Reasonable agreements between the simulation and measurement results are attained. Some slight discrepancies between them may be attributed to measurement errors, inaccuracies in the fabrication process, and the effect of the SMA connector. In this measurement, one port is excited and the other terminated by the standard $50\,\Omega$ matching loads. Considering the symmetry of the four-element antenna, some curves overlap with each other. Regarding the overlaps of the curves, only three curves for simulation and three curves for measurement are needed to be shown. These curves are shown in Figure 8. Because $S_{21}$ and $S_{41}$ are the same, they are not shown in the figure for simplicity. The measured results show that the antenna system covers the frequency bands of 2.4–2.5 GHz, 3.4–3.6 GHz, and 5–5.5 GHz with $S_{11}$ below $-10$ dB. These results show that a good isolation (below $-16$ dB) has been achieved. According to Figure 8, the worst-case isolation for the proposed antenna array is $S_{31} = -16$ dB. The parametric study of $S_{31}$ in terms of antenna-element separation is shown in Figure 9. It is clear according to Figure 9 that the isolation is better than $-20$ dB when the space between antenna elements is less than $0.1\,\lambda$. In comparison with [5] with the same single antenna substrate, this antenna array configuration improved isolation more than 6 dB. In [6], an isolation better than $-17$ dB was achieved for antenna interelement spacing 15 mm or $0.14\,\lambda$, where $\lambda$ is the smallest antenna frequency. In this antenna, an isolation better than $-16$ dB is achieved for antenna spacing 6 mm or $0.048\,\lambda$, where $\lambda$ is the wavelength at the frequency of 2.4 GHz.
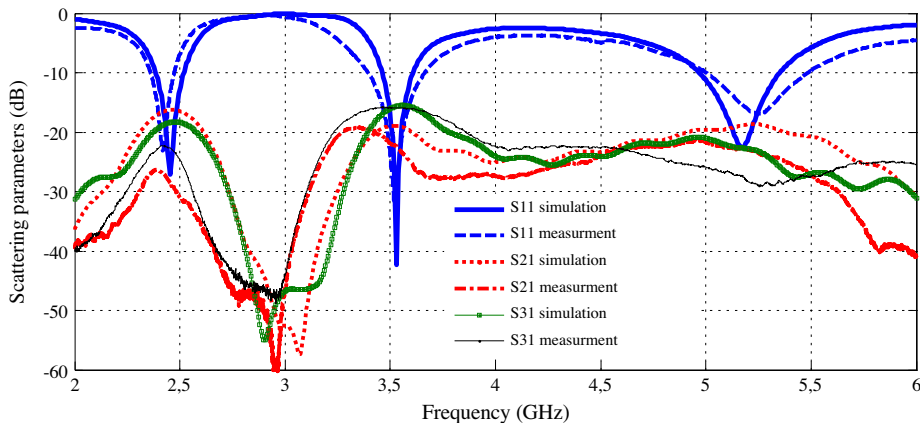


Figure 8.   Simulation and measurement result of *S*-parameters for proposed MIMO antenna.
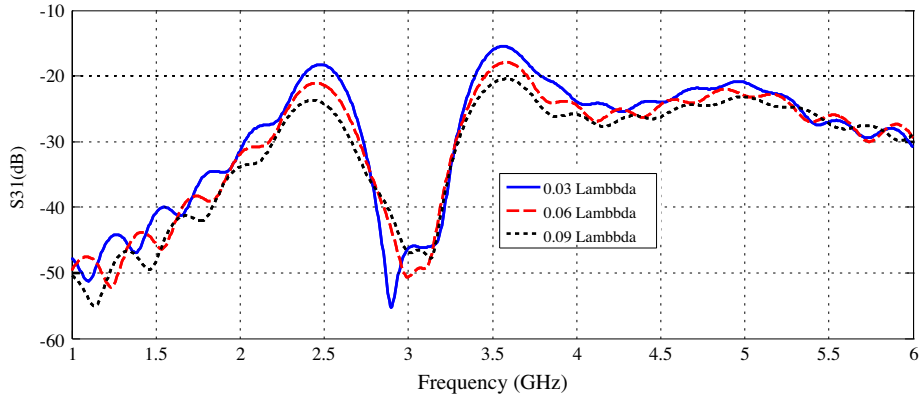
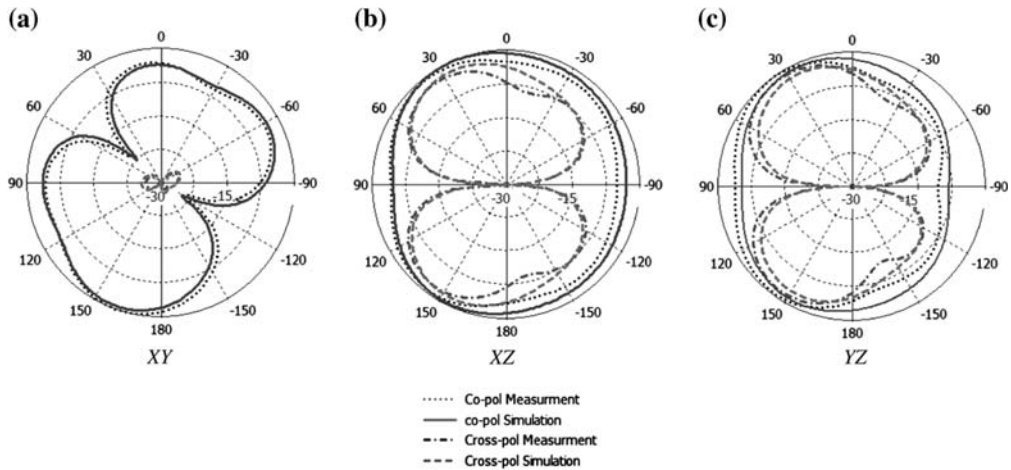Figure 9.   $S_{31}$ variation with different values of antenna separation.



Figure 10.   Simulated and measured radiation pattern of proposed antenna at the frequency of 2.4 GHz for (a) *XY* plane, (b) *XZ* plane, and (c) *YZ* plane.

### 3.2.   *Radiation performance*

Simulated and measured radiation patterns of three principal planes and for three bands of designed frequency, when antenna #1 is fed and the other three antennas terminated by a matching load, are shown in Figure 10–12.

The orientation of the antenna regarding the coordination system is clarified in Figure 1. Both the co- and cross-polarization components are shown. At two planes *XZ* and *YZ*, theta-component is co-polarization and phi-component is cross-polarization. At plane *XY*, phi-component is co-polarization and theta-component is cross-polarization. Nearly omnidirectional pattern in the *XZ* and *YZ* planes and dipole-like radiation pattern in the *XY* plane are obtained at the frequency of 2.4 GHz. At the second and third resonant frequencies, the fixed-size ground plane is electrically larger, so the patterns start to undulate, as well known, because of the larger electrical spacing of diffraction source contributions [19]. However, nearly omnidirectional pattern is achieved at the frequency of 3.5 GHz and 5.2 GHz. There are no deep
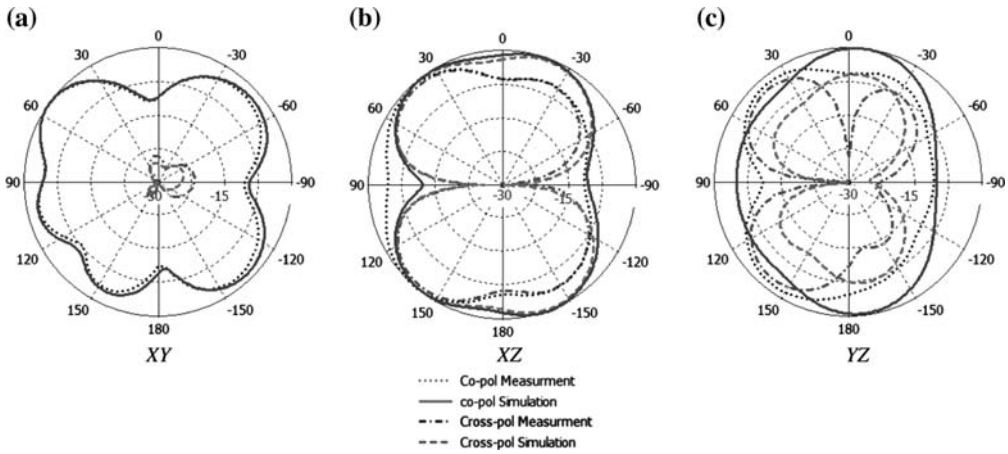
Figure 11. Simulated and measured radiation pattern of proposed antenna at the frequency of 3.5 GHz for (a) *XY* plane, (b) *XZ* plane, and (c) *YZ* plane.
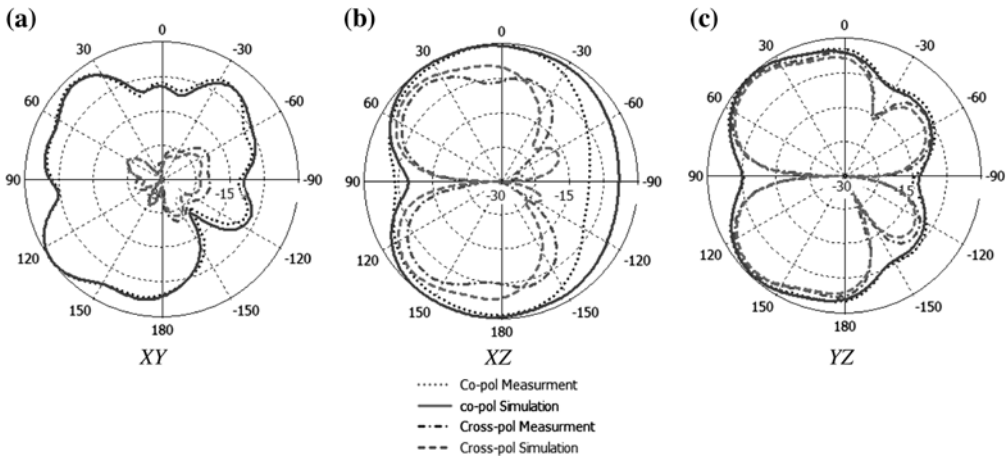


Figure 12. Simulated and measured radiation pattern of proposed antenna at the frequency of 5.2 GHz for (a) *XY* plane, (b) *XZ* plane, and (c) *YZ* plane.

nulls in any direction. This is an important factor when antenna has been used for MIMO application. If the antenna has a deep null in a particular direction that aligns with the direction of the signal's arrival, signal dropouts occur.

### 3.3. Diversity performance

In general, the envelope correlation coefficient of a MIMO antenna can be calculated either through the far-field radiation pattern or via scattering parameters from the antenna. The envelope correlation coefficient can be calculated through *S*-parameters under the assumptions that the incoming signals are uniformly distributed, and the antenna elements are lossless and well matched. The envelope correlation coefficient $\rho_e$ of a four-antenna system can be determined using the following equations [21]:
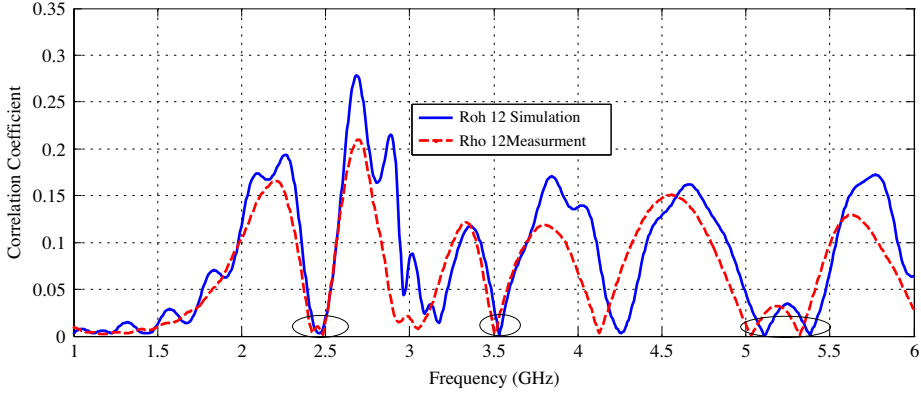
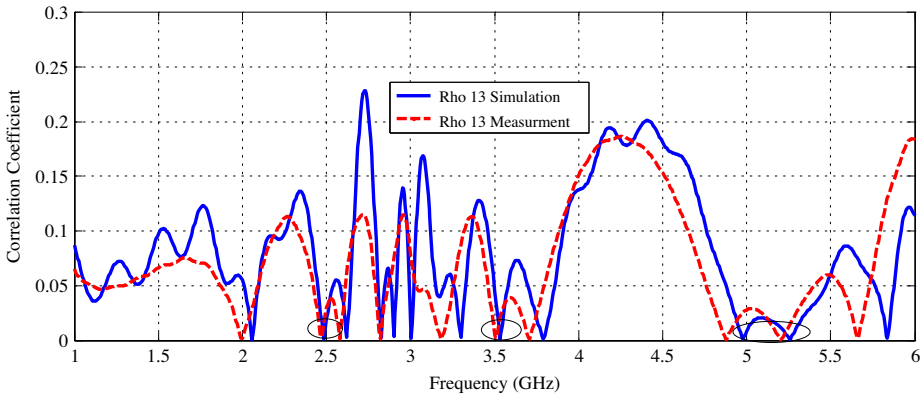Figure 13.   Simulation and measurement results for correlation coefficient between antenna #1 and #2.



Figure 14.   Simulation and measurement results for correlation coefficient between antenna #1 and #3.

$$\rho_{e1} = \frac{\left| S_{11}^* S_{12} + S_{12}^* S_{22} + S_{13}^* S_{32} + S_{14}^* S_{42} \right|^2}{\left( 1 - \left( |S_{11}|^2 + |S_{21}|^2 + |S_{31}|^2 + |S_{41}|^2 \right) \right) \left( 1 - \left( |S_{12}|^2 + |S_{22}|^2 + |S_{32}|^2 + |S_{42}|^2 \right) \right)} \tag{1}$$

$$\rho_{e1} = \frac{\left| S_{11}^* S_{13} + S_{12}^* S_{23} + S_{13}^* S_{33} + S_{14}^* S_{43} \right|^2}{\left( 1 - \left( |S_{11}|^2 + |S_{21}|^2 + |S_{31}|^2 + |S_{41}|^2 \right) \right) \left( 1 - \left( |S_{13}|^2 + |S_{23}|^2 + |S_{33}|^2 + |S_{43}|^2 \right) \right)} \tag{2}$$

where $\rho_{e1}$ and $\rho_{e2}$ are envelope correlations between the antennas #1, #2 and antennas #1, #3 (antenna number is indicate in Figure 1), respectively. The envelope correlation between the antennas #1, #4 is exactly the same as antennas #1, #2. The calculated and measured envelope correlations of the array structure are shown in Figures 13 and 14. The envelope correlation in the interested frequency band is less than 0.05 which is good enough for MIMO applications.

Table 2 shows the simulated peak gain and radiation efficiency. Results show that good gain and high-radiation efficiency (more than 93%) have been achieved for the frequency band of MIMO system.

Table 2.   Peak gain and radiation efficiency results.

| Frequency (GHz) | 2.4 | 3.5 | 5.2 |
|---|---|---|---|
| Peak Gain (dB) | 4 | 4 | 5.8 |
| $\eta$ (%) | 97 | 93 | 99 |

## 4.   Conclusion

A new L-shaped dipole-slot antenna with L-shaped slit has been presented. The L-shaped slot provides two frequency bands at 2.4 GHz and 5.2 GHz, and the third frequency at 3.5 GHz is achieved by introducing an L-shaped slit. The isolation better than $-16$ dB is achieved by separating the common ground plane of MIMO antenna and placing the antennas at the best-array configuration. Relative high gain, envelope correlation less than 0.05, efficiency of higher than 93% and almost omnidirectional patterns at all three frequencies are provided for antenna-array configuration with a low antenna spacing even less than 0.05 $\lambda$. The results show that this antenna array can be a good candidate for MIMO application at the frequency band of WLAN and WiMAX.

## Acknowledgments

## References

[1] Yu XH, Wang L, Wang HG, Wu XD, Shang YH. A novel multiport matching method for maximum capacity of an indoor MIMO system. Prog. Electromagn. Res. 2012;130:67–84.

[2] Ding Y, Du Z, Gong K, Feng Z. A novel dual-band printed diversity antenna for mobile terminals. IEEE Trans. Antennas Propagat. 2007 Jul;55:2088–2096.

[3] Costa JR, Lima EB, Medeiros CR, Fernandes CA. Evaluation of a new wideband slot array for MIMO performance enhancement in indoor WLANs. IEEE Trans. Antennas Propagat. 2011 Apr;59:1200–1206.

[4] Li J-F, Chu Q-X, Guo X-X. Tri-band four element MIMO antenna with high isolation. Prog. Electromagn. Res. C. 2011;24:235–249.

[5] Mohammad Ali Nezhad S, Hassani HR. A novel triband E-shaped printed monopole antenna for MIMO application. IEEE Antennas Wireless Propag. Lett. 2010;9:576–579.

[6] Jusoh M, Jamlos MFB, Kamarudin MRB, Malek MFBA. A MIMO antenna design challenges for UWB application. Prog. Electromagn. Res. B. 2012;36:357–371.

[7] Zhao K, Zhang S, He SL. Closely-located MIMO antennas of tri-band for WLAN mobile terminal applications. J. Electromagn. Waves Appl. 2010;24:363–371.

[8] Wang Z. Reduction mutual coupling of closely space microstrip antenna for MIMO application at 5.8 GHz. J. Electromagn. Waves Appl. 2011;25:399–409.

[9] Cui S, Liu Y, Jiang W, Gong SX, Guan Y, Yu ST. A novel compact dual-band MIMO antenna with high port isolation. J. Electromagn. Waves Propagat. 2011;25:1645–1655.

[10] Li H, Xiong J, He S. A compact planar MIMO antenna system of four elements with similar radiation characteristics and isolation structure. IEEE Antennas Wireless Propag. Lett. 2009;8:1107–1110.

[11] Li J-F, Chu Q-X. Proximity-fed MIMO antenna with two printed IFAS and a wideband T-shaped neutralization line. Prog. Electromagn. Res. M. 2011;21:279–294.

[12] Zhang S, Ying Z, Xiong J, He S. Ultrawideband MIMO/diversity antennas with a tree-like structure to enhance wideband isolation. IEEE Antennas Wireless Propag. Lett. 2009;8:1279–1282.

[13] Addaci R, Diallo A, Luxey C, Thuc PL, Staraj R. Dual-band WLAN diversity antenna system with high port-to-port isolation. IEEE Antennas Wireless Propag. Lett. 2012;11:244–247.

[14] Yu Y, Yuan M, Wu L. A compact printed monopole array with defected ground structure to reduce the mutual coupling. J. Electromagn. Waves Appl. 2011;25:1963–1974.

[15] Najam A, Duroc Y, Tedjni S. UWB-MIMO antenna with novel stub structure. Prog. Electromagn. Res. C. 2011;19:245–257.

[16] Kakoyiannis CG, Constantinou P. Compact printed arrays with embedded coupling mitigation for energy-efficient wireless sensor networking. Int. J. Antenna Propagat. 2010. doi: 10.1155/2010/596291.

[17] Zuo SL, Yin YZ, Zhang ZY, Wu WJ, Xie JJ. Eigen mode decoupling for MIMO loop-antenna based on 180° coupler. Prog. Electromagn. Res. Lett. 2011;26:11–20.

[18] See CH, Abd-Alhameed RA, Abidin ZZ, McEwan NJ, Excell PS. Wideband printed MIMO/diversity monopole antenna for WiFi/WiMAX applications. IEEE Trans. Antennas Propagat. 2012 Apr;60:2028–2035.

[19] Yun JX, Vaughan RG. Open slot antenna in a small ground plane. IET Microw. Antennas Propag. 2011;5:200–213.

[20] Packiaraj D, Vinoy KJ, Kalghatgi AT. Approximate synthesis formulas for microstrip line with aperture in ground plane. Inc. Int. J. RF Microwave CAE. 2012;22:124–130.

[21] Thaysen J, Jakobsen KB. Envelope correlation in (*N, N)* MIMO antenna array from scattering parameters. Microwave Opt. Technol. Lett. 2006 May;48:832–834.